Improved iterative least-squares migration using curvelet-domain Hessian filters

Ming Wang, Shouting Huang, and Ping Wang (CGG)

Summary

Least-squares migration (LSM) can potentially provide better amplitude fidelity, higher image resolution, and fewer migration artifacts than standard migration. Conventional LSM is often solved iteratively through linearized inversion, and therefore is often referred to as iterative LSM. In recent years, various single-iteration LSM approaches have been proposed as a cost-effective approximation of iterative LSM and have produced promising results. To exploit the full potential of LSM, we propose to employ the curvelet-domain Hessian filter (CHF) for single-iteration LSM as a preconditioner for conventional iterative LSM. We call this approach CHF-preconditioned LSM (CPLSM). We first validate our CPLSM approach using SEAM I synthetic data and show that it produces better amplitude fidelity over the single-iteration CHF approach and converges faster than conventional iterative LSM. Furthermore, we demonstrate with an application to field data that CPLSM produces fewer migration artifacts and less noise than conventional iterative LSM. This helps to address a known problem of iterative LSM that is caused by the overfitting of modeled synthetic data (with possibly missing physics) to recorded data.

Introduction

To image the reflectivity of the subsurface, we need to reverse the forward wave-propagation effects with an inverse of the forward modeling operator. Reverse time migration (RTM), the current state-of-the-art imaging technology for complex structures (Baysal et al., 1983; Etgen et al., 2009; Zhang et al., 2009), uses an adjoint modeling operator to approximate the inverse of the forward modeling. The accuracy of this approximation is degraded by spatial aliasing, limited aperture, noise, and non-uniform illumination due to complex overburden (Claerbout, 1992). As a result, the RTM image may have migration artifacts resulting from limited bandwidth and uneven amplitudes.

Least-squares RTM (LSRTM) on the other hand, approximates the inverse of the forward modeling operator through a linearized least-squares inversion by fitting the synthetic and recorded data and can potentially overcome the aforementioned limitations of RTM. The often-cited benefits of LSRTM include more correct image amplitudes due to the ability to compensate for illumination loss caused by complex overburden and limited acquisition setup effects; more coherent images due to the ability to reduce migration artifacts; and higher image resolution due to the LSRTM ability to remove the source signature and source/receiver ghost, as well as migration stretch (Wong et al., 2011; Dong et al., 2012; Dai et al., 2013; Zhang et al., 2013; Zeng et al., 2014). Not surprisingly, LSRTM is being recognized as the next-generation technology for subsalt imaging in the deepwater Gulf of Mexico (GOM) and elsewhere.

However, iterative LSRTM is often prohibitively expensive due to a slow convergence rate (ill-conditioned Hessian matrix for complex structures) and can suffer from migration artifacts and noise due to overfitting of inaccurately modeled synthetic data (inaccurate velocity and inadequate physics used for the modeling process) to the recorded data. Various strategies have been proposed to reduce the computational cost: (1) approximating iterative LSM with single-iteration LSM (Guitton, 2004; Lecomte, 2008; Fletcher et al., 2016; Wang et al., 2016; Khalil et al, 2016), (2) speeding up the convergence rate of iterative LSM through preconditioning of the least-squares inversion (Symes, 2008; Tang and Lee, 2015; Huang et al., 2016), and (3) reducing the number of wave propagations through data-encoding (Dai et al., 2013). Other strategies have been proposed to reduce migration artifacts induced by data overfitting, including a sparse transform of the gradient or the total image (Dutta et al., 2016) and structural smoothing (Dai et al., 2016).

In this study, we extend the CHF operator proposed by Wang et al. (2016) for single-iteration LSM as a preconditioner for iterative LSM to speed up the convergence rate of iterative LSM. In addition, we found that this CHF-preconditioned iterative LSM (CPLSM) can also reduce migration artifacts and noise that are often observed in conventional iterative LSM, thanks to the sparsity constraint used in the curvelet transform and the dip- and frequency-dependent illumination compensation in the curvelet domain.

Theory

Wang et al. (2016) proposed an image-domain single-iteration LSM approach that approximates the inverse of the Hessian matrix with CHF. In this section, we first introduce this CHF approach and then show how to extend the CHF operator to precondition conventional iterative LSM as a second-order optimization problem. During this process, we also explain why the CHF operator is capable of mitigating the two major difficulties discussed above regarding iterative LSM: (1) the slow convergence rate due to ill-conditioned Hessian matrix and (2) migration artifacts and noise due to overfitting the modeled synthetic to the recorded data.

CHF-preconditioned iterative LSM

Image-domain single-iteration LSM: CHF

Data-domain LSM inverts for a reflectivity model, m, to fit the recorded data, d_0 (Tarantola, 1987; Schuster, 1993; Nemeth et al., 1999):

$$f(m) = \frac{1}{2}\|d_0 - Lm\|^2, \quad (1)$$

where $f(m)$ is the cost function to be minimized and L is the linearized Born modeling operator. If L^TL is invertible, the least-squares solution for Equation 1 can be written as:

$$m = (L^TL)^{-1}L^Td_0, \quad (2)$$

where L^T is the migration operator and L^TL is the so-called Hessian matrix, H.

The key to LSM is to find the inverse of the Hessian matrix. Directly computing and inverting the Hessian matrix are impractical for real 3D problems. Following the strategy proposed by Guitton (2004), Wang et al. (2016) proposed to approximate the inverse of the Hessian matrix using a matching filter between the raw image and the demigration/remigration image in the curvelet domain. In this approach, Born modeling is first performed using the migration velocity and the raw migration image, m_0, as a reflectivity model to obtain synthetic data which are then remigrated to obtain a new image:

$$m_r = L^TLm_0. \quad (3)$$

Next, the matching filter s between m_r and m_0 can be found to approximate the inverse of the Hessian Matrix H^{-1} in the curvelet domain by minimizing the following cost function:

$$f(s) = \|C(m_0) - sC(m_r)\|^2 + \epsilon\|s\|^2, \quad (4)$$

where C is the curvelet transform operator, s is the matching filter, and ϵ is a weighting factor for Tikhonov regularization. The output of single-iteration LSM using the CHF approach can be written as:

$$m = C^{-1}\big(|s|C(m_0)\big), \quad (5)$$

where C^{-1} is the inverse curvelet transform operator and $|\ |$ is used to remove the phase, making the matching filter zero-phase, which is important when this approach is extended for surface-offset gathers (Wang et al., 2016).

Using both 3D synthetic and field data, Wang et al. (2016) demonstrated that as a single-iteration LSM approach, CHF can effectively compensate for amplitude loss due to poor illumination caused by complex salt bodies, thus improving the amplitude fidelity of standard RTM. To exploit the full potential of LSM, a gradient-based iterative inversion scheme is still needed. Next, we show how to extend the curvelet-domain Hessian filter s introduced above to precondition conventional iterative LSM.

CHF-preconditioned iterative LSM (CPLSM)

Conventional iterative LSM solves Equation 1 through linearized inversion, in which the gradient can be written as:

$$g = L^T(d_0 - Lm). \quad (6)$$

The convergence of this approach is usually slow because (1) the Hessian matrix is often ill-conditioned, mostly due to unbalanced illumination, and (2) the difference between the modeled synthetic and recorded data is often large due to inaccurate synthetic modeling. One way to improve the method is to use a second-order Gauss-Newton optimization:

$$g = (L^TL)^{-1}L^T(d_0 - Lm). \quad (7)$$

However, as mentioned above, direct computation of $(L^TL)^{-1}$ is impractical for real 3D problems. We can use the CHF operator s defined in Equation 4 as a curvelet-domain approximation of $(L^TL)^{-1}$. The preconditioned gradient can then be written as:

$$g^p = C^{-1}\big(|s|C(L^T(d_0 - Lm))\big). \quad (8)$$

CPLSM can then be formulated as:

$$m_{n+1} = m_n + \alpha_n C^{-1}\big(|s|C(L^T(d_0 - Lm_n))\big), \quad (9)$$

where α_n is the step length calculated by line search:

$$\alpha_n = \frac{(L^TLg^p,\ L^Td_0 - L^TLm_n)}{(L^TLg^p,\ L^TLg^p)}. \quad (10)$$

We note that the image from the first iteration of CPLSM, m_1, is equivalent to the image obtained with the single-iteration CHF approach proposed by Wang et al. (2016), when m_0 is chosen to be zero.

Application to synthetic data

The SEAM I model contains realistic velocity/density contrasts with complex salt geometries that create a variety of illumination issues and thus distort the amplitude response for subsalt events. Figure 1a shows the zero-angle reflectivity model computed from the SEAM I velocity and density models followed by a convolution with a Ricker wavelet of maximum frequency 10 Hz. The amplitudes of subsalt events along all the horizons are fairly uniform. This will be used as a reference to evaluate the amplitude fidelity of different imaging algorithms. The synthetic input data (without surface multiples or added noise) are simulated using acoustic full-wave modeling. The modeling frequency is 10 Hz, the shot grid is 150 m × 150 m, the receiver grid is 100 m × 100 m, and the maximum offset is 8 km in both inline and crossline directions.

In the raw RTM image (m_0) migrated using the true velocity model (Figure 1b), we observe that, compared to the reference in Figure 1a, the amplitudes of subsalt events are relatively weak due to poor illumination caused by the overburden salt. Figures 1c and 1d show images after the first iterations of conventional iterative LSRTM and CHF-preconditioned iterative LSRTM (CPLSRTM), respectively. While both images show improved amplitude response compared to the raw RTM image in Figure 1b, the latter (equivalent to single-iteration CHF) is more effective because the curvelet-domain Hessian filter better handles the dip- and frequency-dependent illumination patterns. Figure 1f shows results after 3 iterations of CPLSRTM. We can see that it further improves the amplitude fidelity over the single-iteration CHF results in Figure 1d, and the CPLSRTM image is also better than the results obtained

after 10 iterations of conventional iterative LSRTM (Figure 1e). This indicates that preconditioning with the CHF operator does improve the convergence rate of iterative LSRTM. Compared to the ground truth in Figure 1a, we can still observe areas (e.g., below the salt in the top-left) where the amplitude distortion is not fully recovered after 3 iterations of CHF-preconditioned iterative LSRTM. We expect that further iterations will improve the results. However, as also observed in other LSRTM approaches, it is very difficult to recover those events with extremely low amplitudes in the raw RTM, and, obviously, impossible to recover completely unimaged events.

GOM field data example

A staggered variable-depth streamer data set from Keathley Canyon, GOM was selected for the field data test. Although known for well-defined salt geometries and overall good images, subsalt images in this area still suffer from uneven illumination, visible migration artifacts, and sub-optimal resolution. The input data underwent typical preprocessing to remove noise, ghost energy, multiples, etc. For this test, we compared standard RTM with 6-iteration conventional iterative LSRTM and 2-iteration CPLSRTM.

Compared to the raw RTM image (Figure 2a), conventional iterative LSRTM (Figure 2b) produced more continuous subsalt events, particularly within the orange circle in Figure 2a. Similar to the results of the synthetic test, subsalt amplitudes in the field data are also more uniform after all the LSRTM approaches (Figures 2b-d). The resolution of the subsalt region in the conventional iterative LSRTM results (Figure 2b) appears to be higher than the raw RTM stack (Figure 2a). However, part of the higher resolution in the iterative LSRTM comes from boosted noise content and migration artifacts that are likely caused by overfitting of some events that were present in the input data but could not be correctly modeled by acoustic Born modeling. We stopped the test at the 6th iteration despite the presence of primary signal still in the data residual, because the noise level continued increasing with the number of iterations.

The single-iteration CHF image (Figure 2c) also shows balanced amplitudes and more continuous events in the subsalt. Unlike conventional iterative LSRTM, CHF did not noticeably alter the vertical resolution or frequency content. This is because we did not model the ghost when generating the demigration/migration image since the input had already been deghosted, and we used a spiky source wavelet for both demigration and migration. As a result, the demigration/migration image (m_r) has similar frequency content to the raw RTM image (m_0). In addition, the design of CHF discourages over-boosting of frequency content with low signal-to-noise ratio (S/N) in the raw RTM image. Alternatively, one can use a band-limited source wavelet (not necessarily a true one) instead of a spiky one in Born modeling and subsequent migrations to broaden the bandwidth through wavelet deconvolution. However, if S/N is low, using a band-limited wavelet will inevitably boost noise as well.

Figure 2d shows the second iteration CPLSRTM results, which have better amplitude fidelity and higher resolution than the single-iteration CHF results (Figure 2c) despite the fact that only 2 iterations were performed. Also, we noticed that the second iteration CPLSRTM has fewer migration artifacts and noise than the second iteration of conventional iterative LSRTM (not shown here) due to the sparsity constraints from the curvelet transform, as well as dip- and frequency-dependent Hessian preconditioning.

Discussion and conclusions

We presented a preconditioned iterative LSM approach that uses the curvelet-domain Hessian filter as a preconditioner. Using both synthetic and field data, we demonstrated that CHF-preconditioning can significantly speed up the convergence rate of iterative LSM and gives better amplitude fidelity with a smaller number of iterations than conventional iterative LSM. In addition, CHF-preconditioning can reduce migration artifacts and noise that are often observed in conventional iterative LSRTM results for field data.

Wang et al. (2016) demonstrated that a single-iteration CHF approach cannot recover completely unimaged events (or those with extremely low amplitudes) in the raw RTM image. A better velocity model and/or a better input data set can provide a better approximation of the inverse of the Hessian matrix and a better initial raw RTM. This also applies to CPLSRTM. In fact, at locations that benefit from the single-iteration CHF approach over the raw RTM, additional uplift is often observed from CPLSRTM. Conversely, if not much benefit is observed in the first iteration, more iterations will likely not help much more.

We showed that CHF preconditioning can be used to mitigate the migration artifacts and noise caused by the overfitting between the inaccurately modeled synthetic and recorded data. On the other hand, it is fundamentally more important to improve the accuracy of our synthetic modeling by improving the velocity model and introducing more physics into our wave propagation such as Q effects (Zhang and Ulrych, 2007; Dutta and Schuster, 2014) and elastic effects (Stanton and Sacchi, 2015).

Tang and Lee (2015) demonstrated that a Hessian approximation based on non-stationary point-spread functions can be used to precondition FWI and thus speed up its convergence and improve the velocity update. The preconditioning scheme based on the CHF operator we described above can be readily extended to FWI as well.

Acknowledgments

We thank SEG for the SEAM I 3D model and CGG for permission to publish this work.

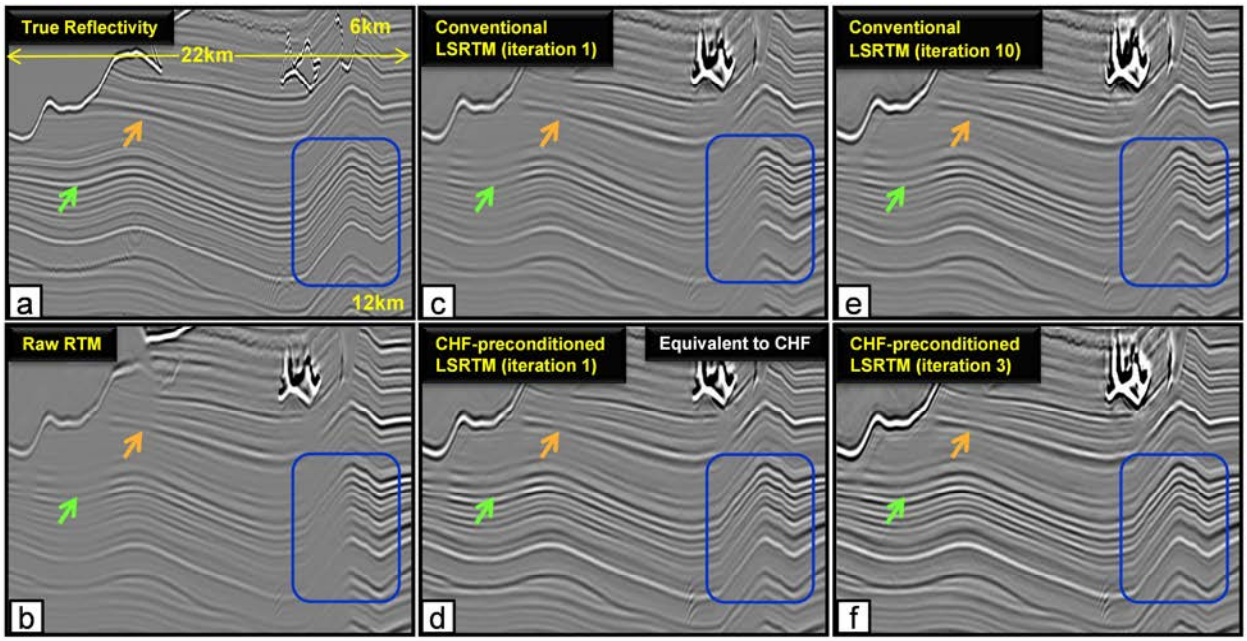

Figure 1: SEAM I synthetic study: Stacked images-(a) true reflectivity; (b) raw RTM using input data after shot and receiver deghosting; (c) image after conventional LSRTM (iteration 1); (d) image after CHF-preconditioned iterative LSRTM (iteration 1); (e) image after conventional iterative LSRTM (iteration 10); (f) image after CHF-preconditioned iterative LSRTM (iteration 3).

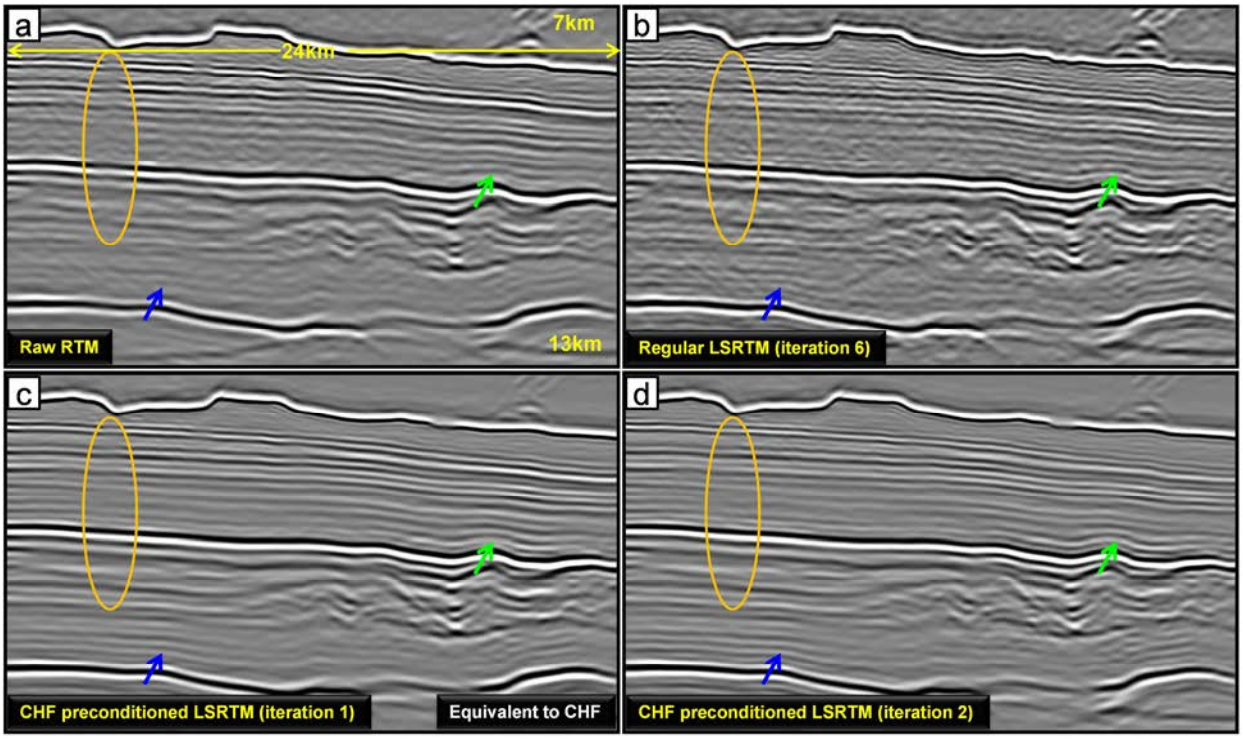

Figure 2: GOM field data example: Stacked images-(a) raw RTM using input data after shot and receiver deghosting; (b) image after conventional iterative LSRTM (iteration 10); (c) image after CHF-preconditioned iterative LSRTM (iteration 1); (d) image after CHF-preconditioned iterative LSRTM (iteration 2)